Tellus (1998), 50A, 333–347
Printed in UK – all rights reserved

TELLUS
ISSN 0280–6495

Analysis of the sea-level variability along the Chinese coast and estimation of the impact of a CO_2-perturbed atmospheric circulation

By MAOCHANG CUI[1] and EDUARDO ZORITA*[,2], [1]*Institute of Oceaonology, Chinese Academy of Science 266071 Quindao, China.* [2]*Institute of Hydrophysics, GKSS Research Centre, 21502 Geesthacht, Germany*

(Manuscript received 15 May 1997; in final form 16 January 1998)

ABSTRACT

The relationship between monthly sea-level data measured at stations located along the Chinese coast and concurrent large-scale atmospheric forcing in the period 1960–1990 is examined. It is found that sea-level varies quite coherently along the whole coast, despite the geographical extension of the station set. A canonical correlation analysis between sea-level and sea-level pressure (SLP) indicates that a great part of the sea-level variability can be explained by the action of the wind stress on the ocean surface. The relationship between sea-level and sea-level pressure is analyzed separately for the summer and winter half-years. In winter, one factor affecting sea-level variability at all stations is the SLP contrast between the continent and the Pacific Ocean, hence the intensity of the winter Monsoon circulation. Another factor that affects coherently all stations is the intensity of the zonal circulation at mid-latitudes. In the summer half year, on the other hand, the influence of SLP on sea-level is spatially less coherent: the stations in the Yellow Sea are affected by a more localized circulation anomaly pattern, whereas the rest of the stations is more directly connected to the intensity of the zonal circulation. Based on this analysis, statistical models (different for summer and winter) to hindcast coastal sea-level anomalies from the large-scale SLP field are formulated. These models have been tested by fitting their internal parameters in a test period and reproducing reasonably the sea-level evolution in an independent period. These statistical models are also used to estimate the contribution of the changes of the atmospheric circulation on sea-level along the Chinese coast in an altered climate. For this purpose the ouput of 150 year-long experiment with the coupled ocean-atmosphere model ECHAM1-LSG has been analyzed, in which the atmospheric concentration of greenhouse gases was continuously increased from 1940 until 2090, according to the Scenario A projection of the Intergovermental Panel on Climate Change. In this experiment the meridional (zonal) circulation relevant for sea-level tends to become weaker (stronger) in the winter half year and stronger (weaker) in summer. The estimated contribution of this atmospheric circulation changes to coastal sea-level is of the order of a few centimeters at the end of the integration, being in winter negative in the Yellow Sea and positive in the China Sea with opposite signs in the summer half-year.

1. Introduction

Sea level is one important environmental parameter concerning coastal ecosystems, harbor building and seawater transport. It is therefore of major concern for the climatologist to try to estimate changes in coastal sea-level that may be associated with an increase of greenhouse-gas forcing in the atmosphere in the future. For this purpose climate models are the only tools to derive the details, in terms of spatial resolution and magnitude, of the expected climate change. These models have been used to estimate large-

* Corresponding author.
E-mail: zorita@gkss.de

scale changes in sea-level due to changes in the oceanic circulation or the volume expansion of sea-water (Mikolajewitz et al., 1990). The degree of confidence put in the results at large-scales is growing (IPCC, 1996).

However such models are limited in their spatial resolution. Even if the grid, which is used for the discretization of the differential equations, is of the order of several hundred kilometers a climate model does hardly offer useful information on that nominally minimum spatial scale. The reason for this failure lies in the inadequate representation of subgrid-scale information, as the details of orography or the coastal configuration, an erroneous parametrization of the physical process that occur at sub-grid scales, and in the disruption of the nonlinear energy cascade at the lowest end of the spectral resolution in the atmospheric models (Von Storch, 1993).

For these reasons, as recognized by the 1995 IPCC report, there exists a large uncertainty in the estimation of the sea-level changes due to a perturbed atmospheric circulation and its potential influence on the modification of the waves, tides and storm climates. Some attempts are now being made to estimate changes in sea-level at local and regional scales by embedding high-resolution regional ocean models into large-scale climate models (Kauker, personal communication), the so called *dynamical downscaling*. Meanwhile other methods, more flexible, such as statistical downscaling (Storch, 1993) have to be used. Within the statistical downscaling framework, the response of a regional variable, in this case coastal sea-level along the Chinese coast, to large-scale climate forcing is described by a linear model, the parameters of which are fitted using available observations. Once the model has been set up, it can be used to reconstruct past variations of the regional variable if large-scale observations extending longer back into the past are available, or to estimate possible regional changes under a perturbed climate using the output of climate change experiments with coarse-resolution climate models. The statistical models, therefore, try to model in one step the chain of causes and effects that lead from the monthly mean large-scale circulation through the atmospheric transients and wind-stress, waves, tides, rainfall, etc., to local sea-level anomalies. The local peculiarity are taken into account by fitting their internal parameters to observed data sets. This statistical approach has been already applied to coastal sea-level in the Baltic Sea (Heyen et al., 1996) and at the Japanese Islands (Cui et al., 1995).

It has to be noted that the validity of the statistical model cannot be guaranteed in a perturbed climate. The parameters of the model have been fitted using the natural variability of the observed climate and it can be only expected that this natural variability contains a great variety of atmospheric situations. The statistical model will hopefully identified those situations that are relevant for coastal sea-level and be able to translate changes in the frequency or intensity of this perturbed atmospheric forcing into coastal sea-level changes. Strictly, a statistical model is only valid as long as the mean climate changes do not exceed the level of the natural variability of the observed climate, which is the case for mean climate change simulated by the present General Circulation Models. In some sense this problem is also present in dynamical downscaling or the GCMs themselves, since the parametrizations that represent local processes in these models have been empirically formulated using just present observations.

For the design of a reasonable statistical model, some previous (physical) reasoning about the physical factors affecting coastal sea-level is required. Three groups of processes may be important in this respect: the geological processes, the regional-scale dynamical processes and the large-scale dynamical processes (Patullo et al., 1955; Lisitzin and Patullo, 1961; Gill and Niiler, 1973; Wyrtki, 1990). The geological processes are normally very slow (except in the case of earthquakes) and may be treated as linear, or even absent, on time scales of years or decades. If we subtract the linear trends from the local sea-level, these processes will efficiently be filtered out. The volume expansion of sea water and the melting of glaciers due to possible global warming (Warric and Orlemans, 1990), the changes in the barotropic mode of the large-scale ocean circulation, as well as human water pumping activities from the subsoil (Sahagian et al., 1994) are other large-scale, and quite probably slow and linear, factors affecting coastal sea-level. If this effect has already entered into play, it can be also filtered out by linear detrending the data set. More relevant in this context are the regional scale processes, such the inverse barometric effect of more or less air pressing on the surface of the ocean, the steric effect of the water column being more or less dense (as a consequence of changing temperature and the effects of the regional oceanic and atmospheric circulations). More locally, for instance, near a river-mouth the streamflow will influence the local tide gauge, specially for large rivers such as the Yangtze. Of course, once the influence of the local processes has been estimated, all these effects, geological, large-scale and regional, have to be added up for a complete estimation of possible sea-level changes.

The accuracy with which these regional processes are simulated in present-day climate models (with typical horizontal resolutions of 5°) varies considerably. The inverse barotropic effect depends only on the large-scale atmospheric pressure and is therefore likely well simulated. The steric effect depends on such regional effects as the cloud cover or the availability of mixing energy, which is less well described by atmospheric models. The effects of local ocean currents, local coast lines and streamflows are normally not included in such models.

1.1. Possible factors affecting Chinese coastal sea-level variability at monthly time scales

The Chinese coast is connected to a broad and shallow land sill with an average water depth of only about 20 m and the typical magnitude of sea-level variations at monthly time scales is of the order of 50–100 mm. One important factor for sea-level variability is obviously the effect of wind-stress, either by direct pile-up of water, anomalous Ekman transport, or through the dynamical equilibrium with the Coriolis force acting on currents. Since this effect depends strongly on the coastal topography and momentum flux to the ocean, its magnitude is difficult to estimate. The magnitude of the inverse barometer effect has been found to be nearly the equilibrium response of sea water to atmospheric pressure (Wunsch and Stammer, 1997), namely 1 cm $\sim$ 1 mb. Typical anomalies of monthly atmospheric pressure are of the order of 2 mb, so that the inverse barometer effect could in principle cause sea-level anomalies of 20 mm. Anther factor is the volume expansion of water caused by temperature variations. The monthly variability of the water temperature anomalies in the mixed layer is typically of the order of 1°C. Since the volume expansion coefficient of seawater is approximately $2.5 \times 10^{-4}\,C^{-1}$ the expected sea-level anomalies caused by the steric effect could be also of the order of 20 mm. These figures are just rough estimations of the relative order of magnitude of the different factors. The sea-level anomalies actually observed are of course the result of the interplay of all these factors, which presumably depend on the local peculiarities of each gauge station.

1.2. Selection of the large-scale forcing

For the formulation of a statistical downscaling model we have to resort to large-scale variables that satisfy two conditions: First, sufficiently long homogeneous time series available to fit the model parameters with observed data are needed. Second, the forcing must be well simulated by climate models. The latter condition limits the set of candidates to large- scale or regional-scale fields (with a scale of a 1000 km or more), such as sea-surface temperature, sea-level pressure or geopotential height at some level. One has to be aware, however, of the limitations of such a selection. The East Chinese coast is exposed to an important seasonal phenomenon, namely the East Asian Monsoon and its associated intense rainfall. It is known that the summer monsoon always appears first in East Asia, usually in the middle of May, before the Monsoon development over the Bay of Bengal during late May and over the western coast of the Indian subcontinent in early June. In East Asia the earliest onset line occurs in the northern South China Sea, and extends to the western Pacific east of Taiwan and south of Japan. The onset date progresses northward and northwestward. By mid-June the East Asia Monsoon is characterized by the abrupt intensification of rainfall along the Yangtze river, then extending into Japan. The rain-belt moves abruptly into north China in mid-July (Tao and Chen, 1987). About 80% of the total annual precipitation in China occurs following this mean Monsoon evolution.

However, the interannual variability is very large (Lau et al., 1988). Therefore it is expected that the Monsoon may exert some influence on the coastal sea-level variability. The reverse situation, i.e., years with anomalously low rainfall should be associated with lower than normal coastal sea-level, at least in the stations located in the basin of large rivers.

It cannot be expected that coarse-resolution climate models simulate properly a phenomenon as complex as the Monsoon, where the atmospheric circulation, SSTs, topography, and precipitation interact with complicated and not completely understood feed-backs. Statistical models will be able in principle to describe only in a crude way the relationships between SLP and SST in one side, and rainfall and sea-level on the other side. Therefore, the downscaling results of the GCM simulations in the Monsoon season should be considered with more care.

This paper is organized as follows: in Section 2 the observational data set used in this study are described. In Section 3 the strategy for the formulation of the statistical model is presented. In Section 4 the results of the Canonical Correlation Analysis between coastal sea-level and sea-level pressure and sea-surface temperature is analyzed and the validity of the resulting statistical model is tested. In Section 5 the downscaling model is applied to interpret the output of a climate change experiment, thus estimating the contribution to future coastal sea-level changes by these forcing fields. The paper is closed with concluding remarks in Section 6.

2. Data

In this study, we examine monthly mean values of sea-level along the Chinese coast, of sea surface temperature and of sea-level air-pressure data in the West Pacific and South China Sea and of sea-level air-pressure data over China.

• The local sea-level data at 19 stations along the Chinese coast for the period January 1960 through December 1990 have been compiled by the Marine Scientific and Technological Data Center at partial coastal stations run by State Oceanic Administration in China. The positions of the 19 tide gauges are given in Fig. 1 together with their names in Table 1.

• Fields of monthly sea-level pressure over China (15°N–55°N latitude, 70°E–140°E longitude, see for instance Fig. 3) were available on a 5° × 5° grid. Such fields, which have been prepared by the National Center For Atmospheric Research (NCAR) in Boulder, USA, are available for the time interval January 1960 until December 1990.

• For some testing calculations rainfall data were also used. These data were prepared as monthly means gridded field (2.5° longitude × 3.5° latitude over East China (20°N–45°N,

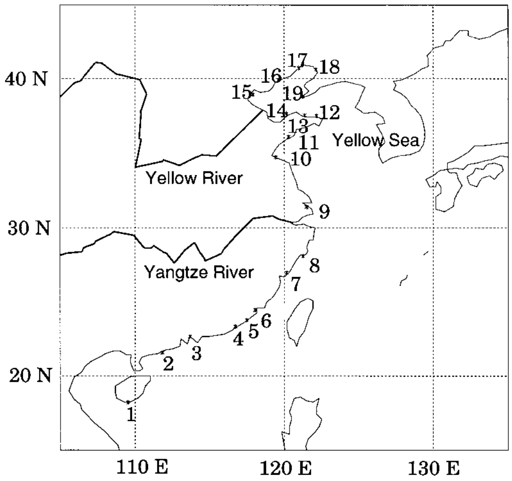

Fig. 1. Positions of the gauge stations used in this study. The Yellow and Yangtze rivers are also schematically shown.

Table 1. *Names of the gauge stations used in this paper*

Station number	Station name	Longitude	Latitude
1	Yulin	109.51	18.21
2	Zhapo	111.83	21.58
3	Huangpu	113.45	23.1
4	Shantou	116.73	23.33
5	Dongshan	117.50	23.78
6	Xiamen	118.06	24.45
7	Sansha	120.16	26.96
8	Kanmen	121.26	28.08
9	Wusong	121.50	31.38
10	Lianyungan	119.45	34.73
11	Qingdaodagang	120.3	36.08
12	Weihai	122.16	37.50
13	Yantai	121.38	37.53
14	Longkou	120.16	37.65
15	Tanggu	117.91	38.93
16	Qinuangdao	119.61	39.91
17	Huludau	120.98	40.71
18	Yingkou	122.13	40.61
19	Lushun	121.25	38.8

99.5°E–125°E)) by the UK Department of Environment for the time interval January 1960–December 1990.

The data have been processed in the following steps.

- The Chinese coast is tectonically active. Since 1950 trends of coastal sea-level with different signs have been reported along the Chinese coast (Wang, 1986). The coast near Wusong and Lianyungang rises at a rate of about 5.4 mm/year. But the coast in Jiangsu and Sandong Provinces is rather stable and the coast in other regions sinks with a rate from 8.1 to 10.5 mm/year. It is noticeable that the coast of Tanggu sinks at a rate of up to 46 mm/year after the earthquake in 1976 in Tangsan (Wang, 1986). These rates are estimated mainly from the sea-level data itself so that we cannot correct the sea-level data with these estimates to "clean" the data from tectonic influences. It seems reasonable to assume that these slow tectonic processes that are not directly related to climate, as well as others such as land subsidence by local hydrocarbon mining activities, can be filtered out from the sea-level data by subtracting the long-term linear trend. However the typical observed trends are small compared to the natural monthly variability. Fig. 2 shows the raw monthly sea-level at station 12 (Weihai, the time series of which can be considered as typical). Since the linear trend can also contain the influence of low-frequency climate variability, the climate time series were also detrended for a consistent statistical analysis.
- The anomalies of all data were calculated by subtracting the long-term annual cycle.

3. Formulation of the statistical model

The methodology to specify the statistical model linking coastal sea-level and large-scale climate forcing follows closely the one described by Cui et al. (1995) for the Japanese Islands and Heyen et al. (1996) for the Baltic Sea. A detailed technical description has been given by Bretherton et al. (1992). Therefore, only a brief summary is given here. The anomalies of the large-scale (gridded) forcing $\boldsymbol{L}(t)$ and the response of the local variable $\boldsymbol{R}(t)$ are decomposed in a series of patterns:

$$\begin{aligned} \boldsymbol{L}(t) &= \sum_{i=1}^{n} \alpha_i(t)\boldsymbol{p}^i, \\ \boldsymbol{R}(t) &= \sum_{i=1}^{n} \beta_i(t)\boldsymbol{q}^i, \end{aligned} \tag{1}$$

where $\boldsymbol{p}^i$ and $\boldsymbol{q}^i$ are time independent spatial patterns and $\alpha_i(t)$ and $\beta_i(t)$ are time series that can be defined to have standard deviation equal to 1. We use canonical correlation analysis (CCA) to find the optimal decomposition of both fields. The result of CCA are time series $\alpha_1(t)$ and $\beta_1(t)$ with show the highest correlation. The following pair $\alpha_2(t)$ and $\beta_2(t)$ shows the highest correlation with the additional constraint that they are uncorrelated with $\alpha_1(t)$ and $\beta_1(t)$, respectively. The patterns $\boldsymbol{p}^i$ and $\boldsymbol{q}^i$ are called the canonical patterns, the associated time series $\alpha_i(t)$ and $\beta_i(t)$ are the canonical time series, and the correlation between them are called the canonical correlations. Based on this analysis an optimized regression equation linking the canonical time series can be formulated. The estimation of the anomalies of the local variables conditional on a given large-scale forcing, as observed from another period or simulated by a GCM, is performed by calculating the new amplitude of the time series $\alpha_i(t)$ in the forcing and estimating the time series $\beta_i(t)$ through the regression equation. The physical magnitude of the local anomalies can be finally estimated by eq. (1).

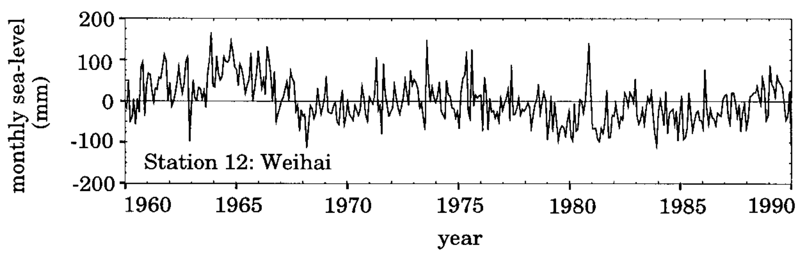

Fig. 2. Undetrended time series of monthly sea-level anomalies at station 12 (Weihai).

4. Canonical correlation of sea-level pressure and coastal sea-level

The canonical correlation analysis of sea-level variations at the 19 Chinese stations and the sea-level pressure anomalies over East Asia China has been performed separately for the winter and summer seasons. The selection of the months belonging to each of the half years is based on the importance of the Monsoonal circulation in the area. As explained in the introduction rainfall associated with the East Asian Monsoon starts in May in the South and can be considered to be finished in August–September in the north. Therefore, we have defined the summer season as the months May through September, and the winter season as the remaining months.

In both cases the statistical analysis between sea-level and sea-surface temperature (SST) in the western Pacific yielded no clear association, and was weaker that those found between sea-level and atmospheric sea-level pressure (SLP). This is consistent with the known fact that the physical connection between both fields, SST and SLP at mid-latitudes, is due to the active role of the atmospheric anomalies in generating SST anomalies (by air-temperature advection, especially in wintertime, and by Ekman pumping) (Lau, 1997). For these reasons the associations between SST and sea-level were not investigated further, since it was assumed that the possible relationships between SST and sea-level through the steric effect would be overshadowed by the direct influence of the atmosphere on sea-level.

4.1. Winter half year: October through April

In winter, two pairs of patterns which are strongly connected (correlations of 0.71 and 0.50), and that represent about 35% and 20% of the total sea-level variance can be identified (Fig. 3). The first pattern describes SLP anomalies that are associated with anomalies of the geostrophic wind blowing along the Chinese coast. The coastal sea-level anomalies related to this pattern are negative in the stations located within the Yellow-Sea basin (Fig. 1) and positive in the rest, exposed to the open ocean. The association between both patterns is physically consistent with water being flushed out from the Yellow Sea by the anomalous wind stress and an enhanced Ekman transport into the Chinese coast. The advection of cold air masses from the continent and the subsequent cooling of the Yellow Sea may also contribute, but both effects are difficult to separate in this region.

The second SLP pattern shows negative anomalies in the Northwest of China and positive anomalies over much of south and central China. The geostrophic wind anomalies associated with this SLP pattern are directed from the continent to the Pacific Ocean. The sea-level pattern is positive almost everywhere, except in the stations in the Yellow Sea. The most plausible physical explanation for this second pair is the inverse barometer effect. Although there exists dynamical components associated with this effect, at these time scales the relationship between the local SLP and sea-level is quite approximately 1 mb $\sim$ 1 cm (Wunsch and Stammer, 1997), which agrees reasonably well with the second pair in Fig. 3. Other possible mechanisms, such as the steric effect, would yield relationship between SLP and sea-level of the opposite sign as the ones represented by this second canonical pattern. For instance, the SLP pattern is associated with cold air-mass advection from the continent, which should reduce the sea-level in the Yellow Sea.

The validity of the statistical relationship identified by the CCA has been tested by performing the analysis with the data from the period 1960–1975 and by trying to reconstruct the sea-level anomalies using the SLP observations in the period 1976–1990, as explained in the previous Section. The resulting sea-level anomalies in the winter season for three representative stations (stations 5, 8 and 12 in Fig. 1) are shown in Fig. 4. One can see that the agreement between reconstructed sea-level anomalies and the observations improves for the three stations (linear correlations of 0.42, 0.40 and 0.52, respectively). This results supports the initial hypothesis that to a great extent the sea-level variability along the whole coast is caused by the direct influence of the atmosphere on the sea-surface.

4.2. Summer half year: May through September

A similar canonical correlation analysis has been performed for the summer months (April–September). The SLP canonical patterns obtained in the summer season (not shown) are different

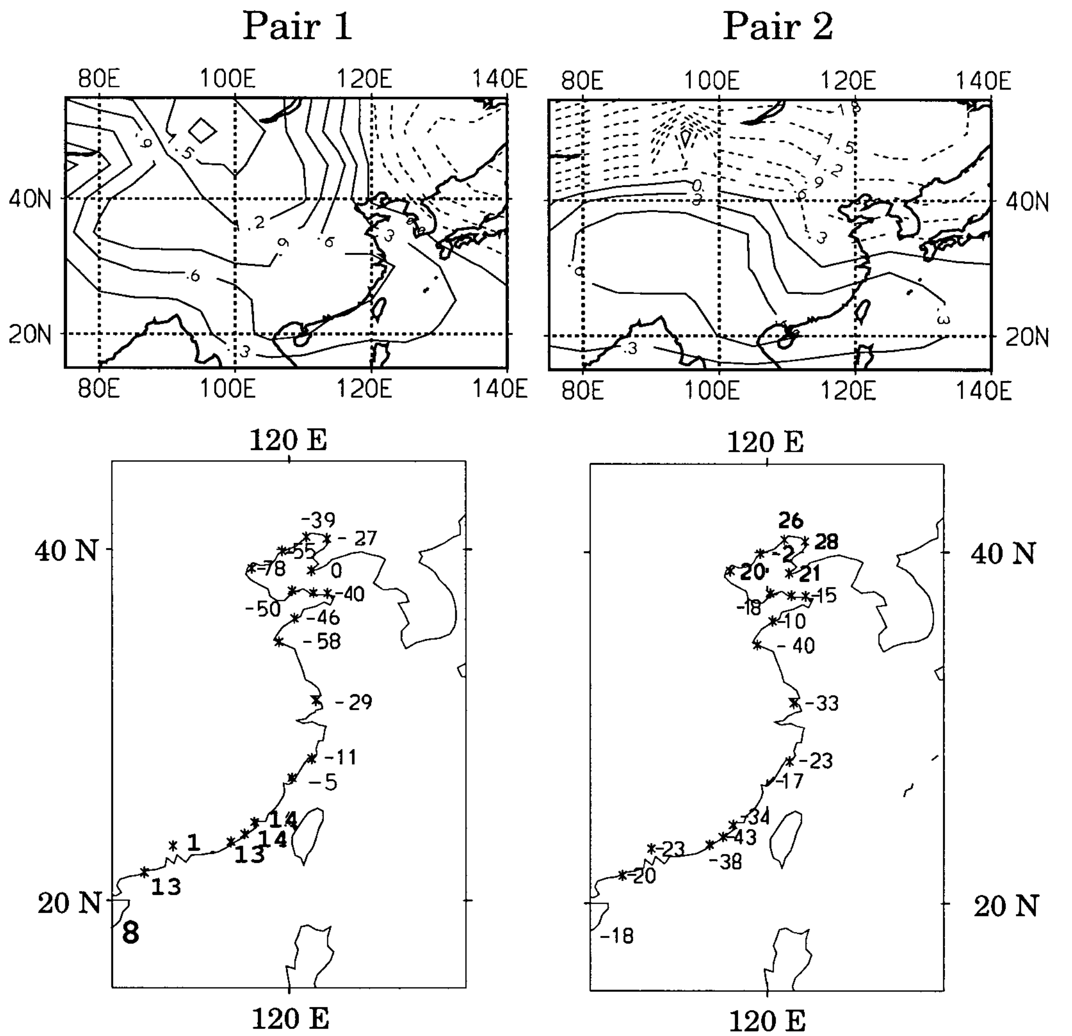

Fig. 3. The two leading canonical correlation pairs of SLP (hPa) and sea-level anomalies (mm) in the winter season (October–April). The correlation between the corresponding time series is 0.71 and 0.50, respectively. The variance explained by the sea-level patterns is 33% and 19%, respectively. Dashed contours are negative.

from those in the winter season, as the typical circulation patterns are also different. The first SLP pattern has a north-south dipole structure with a high pressure cell sitting over the Yellow Sea and low pressure over the South-Western Pacific off the Chinese coast. The associated geostrophic circulation anomaly is oriented zonally.

The second SLP pattern represents a weaker west-east dipole with associated meridional geostrophic circulation anomalies. The sea-level variance explained is 25% and 12%, respectively.

To further investigate the reasons for this low explained variance, the canonical correlation analysis was performed in half of the period available (1960–1975) and the sea-level anomalies in the remaining period (1976–1990) were reconstructed from the SLP observations. The results for the stations 5, 8 and 12 are shown in Fig. 5. It can be seen that whereas the reconstructed sea-level anomalies agree reasonably well in stations 5 (south, linear correlation of 0.38) and in station 8 (intermediate, linear correlation of 0.48), the sea-

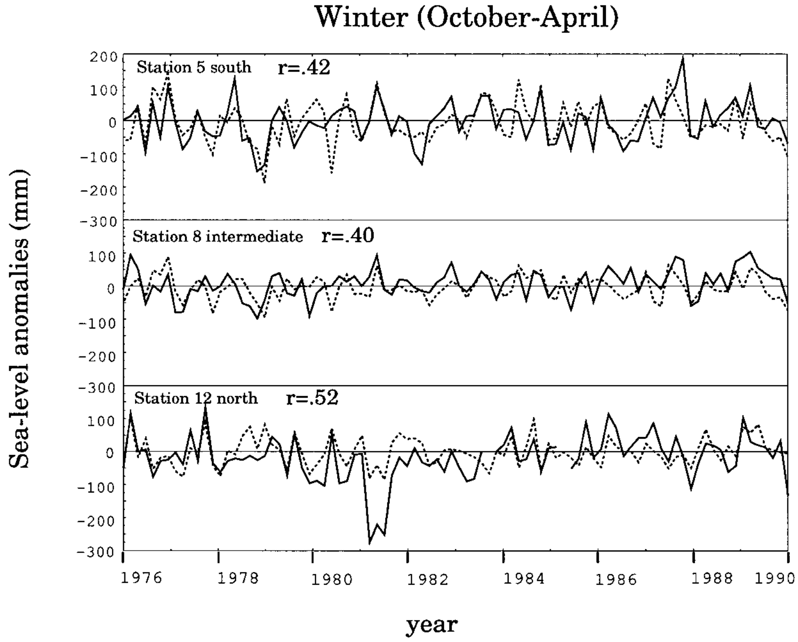

Fig. 4. Observed (solid) and reconstructed (dashed) monthly sea-level anomalies in stations 5, 8, 12 (Fig. 1) in winter (October–April). The reconstruction is based on the simultaneously-observed SLP anomalies and the statistical model based on the Canonical Coprrelation Analysis. *r* denotes the linear correlation betwwen observations and reconstruction.

level reconstruction is very poor in the north (station 12, linear correlation of 0.16). Also the reconstructed level of variability is much smaller than in the observations. This suggests that in the summer season, the patterns of the atmospheric circulation relevant for coastal sea-level may be considerably different in the Yellow Sea than in the rest of the Chinese Coast.

Therefore, the stations were divided into 2 groups, the Yellow Sea group (group YS, stations 10–19) and the rest (group R) and the analysis was repeated for two groups separately. The CCA analysis for the group R identifies just one pair of pattern, shown in Fig. 6. The SLP pattern has a dipole structure with negative anomalies over the Western Pacific and positive anomalies over the Yellow Sea. The coastal sea-level anomalies in the China Sea are all positive. This relationship can be reasonably explained by anomalous Ekman upwelling under the low-pressure cell. The CCA of coastal sea-level in the Yellow Sea and SLP is not able to identify any pair of patterns in the summer months that are significantly correlated. However, the EOF analysis of YS sea-level indicates that just one single mode is able to describe about 50% of variance, having the same sign over all YS stations. Due to the particular characteristics of the coastline it may be possible that the SLP pattern that forces the sea-level is not contained in the leading EOFs of SLP in this area.

To further investigate this hypothesis, the regression pattern of the first YS sea-level principal component and the SLP field was calculated (Fig. 7). The SLP describes in fact geostrophic circulation anomalies that should be connected to a flushing out of water into the Yellow Sea. This associated SLP pattern is effectively not contained in the subspace spanned by the leading SLP EOFs and actually projects strongly in one of the higher order EOF patterns (not shown). This fact may shed some doubts about the physical significance of this associated SLP pattern and therefore onto the SLP-sea-level relationship in the Yellow Sea. To ascertain the physical significance, we have calculated the regression pattern between the YS sea-level principal component and rainfall in

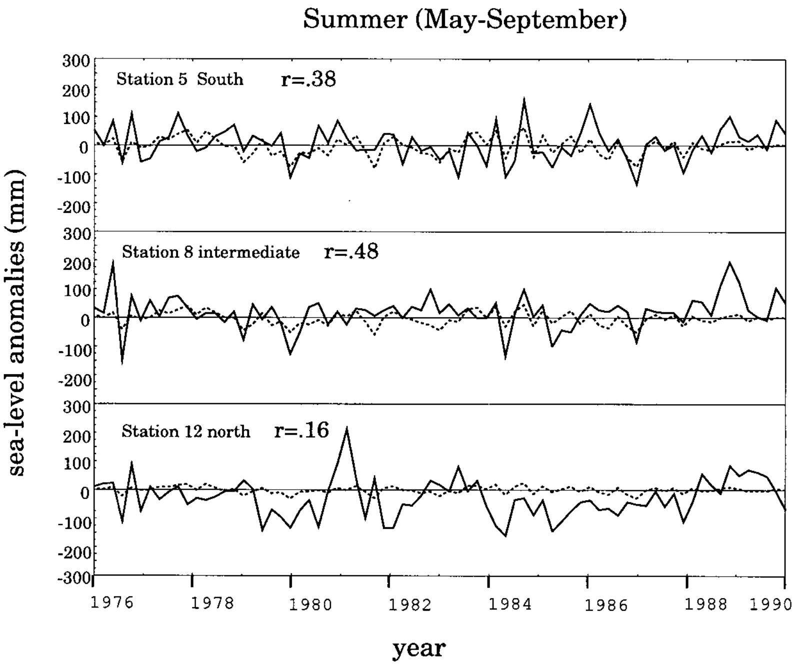

Fig. 5. Observed (solid) and reconstructed (dashed) monthly sea-level anomalies in stations 5, 8, 12 (Fig. 1) in summer (May–September). The reconstruction is based on the simultaneously-observed SLP anomalies and the Canonical Correlation Analysis for all stations simultaneously. *r* denotes the linear correlation between observations and reconstruction.

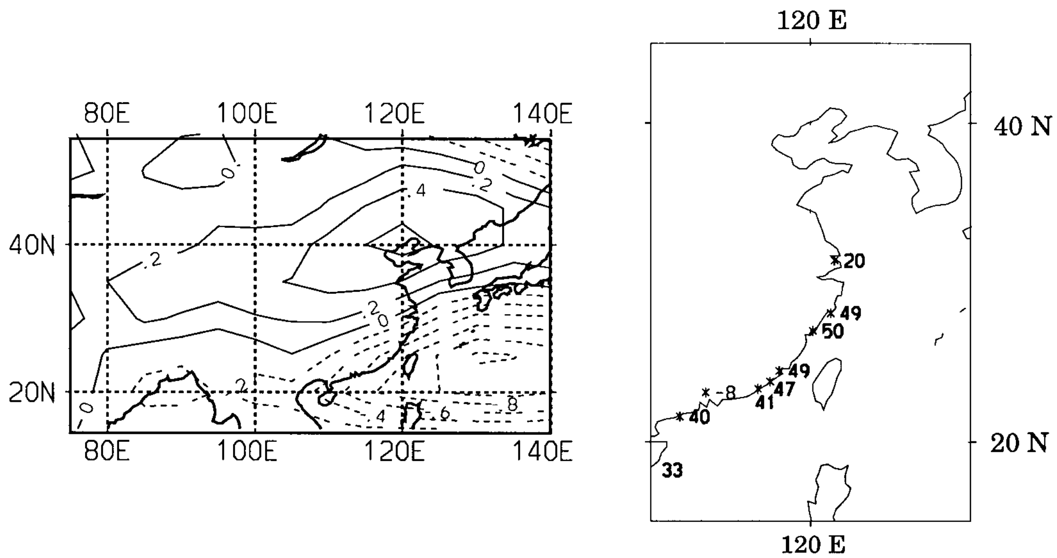

Fig. 6. The leading canonical correlation pair of SLP (hPa) and sea-level anomalies (mm) in the Southern stations in the summer season (May–September). The correlation between the corresponding time series is 0.72 and the variance explained by the sea-level pattern is 45%. Dashed contours are negative.

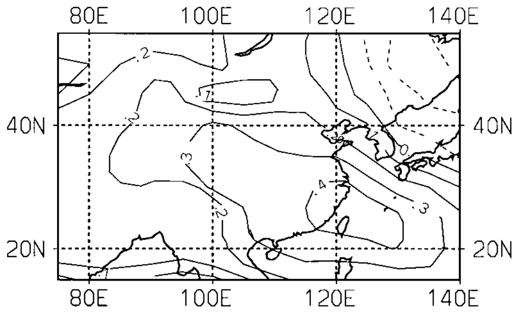

Fig. 7. The SLP regression pattern in the summer season (May–September) based on the first principal component of Yellow Sea coastal sea-level. Units are hPa. Dashed contours are negative.

China in the summer season. Our reasoning is that if the associated SLP pattern of Fig. 7 bears a real physical significance, it should also have a fingerprint not only in the YS sea-level, from which it was derived, but also in the rainfall anomalies. This fingerprint should then also appear in the rainfall regression pattern, which is shown in Fig. 8.

The rainfall regression pattern describes weak positive anomalies in most parts of Central China and South China and negative anomalies along almost the whole East coast and in the Yellow Sea. One can see that the rainfall regression pattern and the SLP regression pattern in Fig. 7 are reasonably physically connected: in summer time the geostrophic wind anomalies should bring moist air masses into the continent, while the high pressure cell sitting at the west coast inhibits the rainfall. This supports the physical existence of the SLP pattern in Fig. 7 as forcing for the YS sea-level in summer.

The statistical model describing the connection between SLP and coastal sea-level is then separately formulated for the YS stations and for the R stations. For the R group, the canonical SLP of Fig. 6 is taken, while for the Yellow Sea the associated SLP pattern of Fig. 7 is used. To test the model the same calculations as described in this Subsection have been performed for the subperiod 1960–1975, and the corresponding SLP and sea-level patterns have been calculated. The model is then used to reconstruct the sea-level anomalies in summer for the subsequent subperiod 1976–1990. The results for the three representative stations is shown in Fig. 9.

The agreement between reconstructed and observed sea-level anomalies is better that before for all three representative stations (linear correlation coefficients of 0.47, 0.55 and 0.35, respectively).

It is concluded that the agreement between observed and reconstructed sea-level anomalies in winter and summer, shown in Figs. 4 and 9 lends support to the use of these statistical models to estimate future sea-level changes caused by slow changes of the atmospheric circulation due to anthropogenic greenhouse-gas forcing.

5. Estimation of coastal sea-level changes under future anthropogenic greenhouse gas forcing

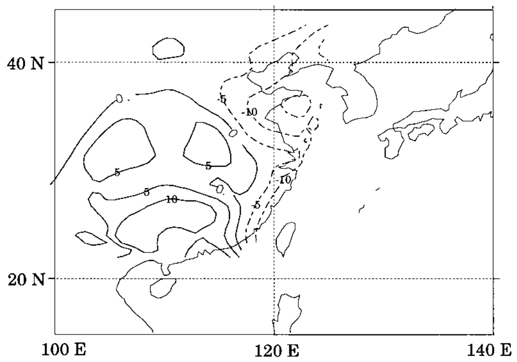

Fig. 8. The rainfall anomalies regression pattern in the summer season (May–September) based on the first principal component of Yellow Sea coastal sea-level. Contour interval is 5 mm/month. Dashed contours are negative.

The statistical relationship between SLP and coastal sea-level can be used not only to reconstruct past variation of sea-level but also to estimate future changes under different greenhouse forcing scenarios. For this purpose the changes of the atmospheric circulation simulated by a General Circulation Model (GCM) can be used as input for the statistical model.

In this section one integration with the ECHAM1-LSG coupled climate is analyzed. The ECHAM1 atmospheric model is a spectral model with an equivalent horizontal resolution of about 5.6° and 19 levels in the vertical. The LSG ocean model has an effective horizontal resolution of about 4.2° and 11 levels. In this integration the observed concentration of atmospheric green-

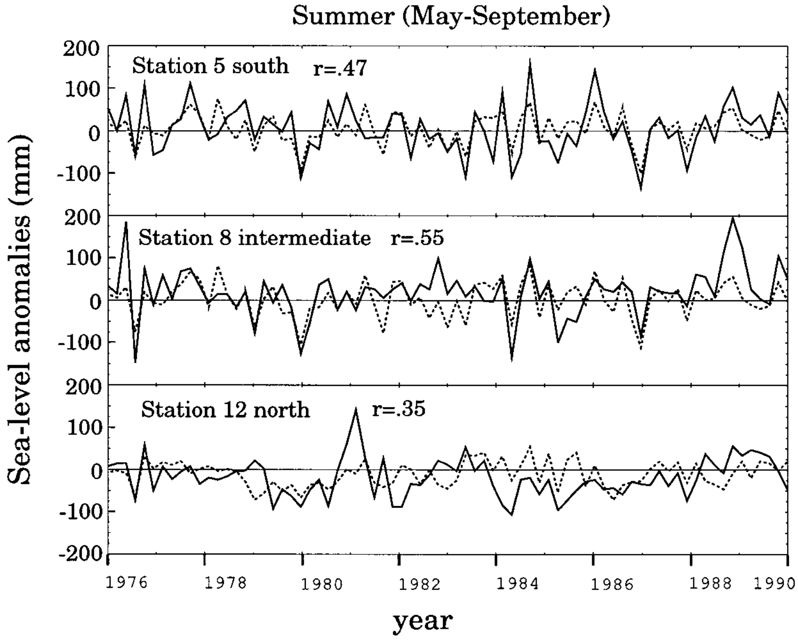

Fig. 9. As in Fig. 5, but based on a separate statistical model for the Yellow Sea stations and the rest of Chinese stations. *r* denotes the linear correlation betwwen observations and reconstruction.

house gases between 1940 and 1985 was prescribed as observed. From 1986 onwards the model was forced by greenhouse gas concentrations according to the Scenario A of the Intergovernmental Panel on Climate Change (IPCC, 1990), which corresponds roughly to a yearly increase of 1.3% of the effective CO_2 concentration. The effective CO_2 concentration is therefore doubled at year 2035 of the integration with respect to the concentration in year 1985. Additional details over this coupled climate model can be found in Cubasch et al. (1992) and of this transient experiment in Cubasch et al. (1995).

The SLP anomalies from this experiment were calculated by subtracting the *simulated* mean annual cycle for the same period in which the statistical model was fitted, namely 1960–1975. In this way the systematic errors of the climate model are subtracted out.

The SLP patterns on which the two seasonal statistical models are based evolve differently in the Scenario A integration. This is shown in Fig. 10, where the amplitudes of these patterns along the period of integration is depicted (to underline the low-frequency evolution the time series were seasonally averaged). The trends in all four cases are clearer from roughly the year 2050 onwards, where the effects of the additional greenhouse gas forcing should be more apparent. Concerning the winter SLP patterns, the amplitude of the 1st (2nd) SLP pattern (Fig. 3) tends to become more negative (positive) at the end of the integration, which means that the SLP contrast between the Asian continent and the Pacific Ocean tends to become weaker, leading to weaker winter Monsoon circulation. On the other hand the zonal circulation, represented by the second canonical pattern becomes more active in winter. In the summer season, the leading canonical pattern (Fig. 6) becomes stronger, which means that the westerlies over China in this season are weakened. Contrary to this, the more local pattern associated with the sea-level variability in the Yellow Sea gets stronger in the last decades of the integration, leading in this area to a more meridional (northerly) atmospheric circulation.

It may be therefore concluded that in the future climate simulated by the ECHAM1-LSG model the atmospheric circulation over China will tend to be more zonal in the winter season and more

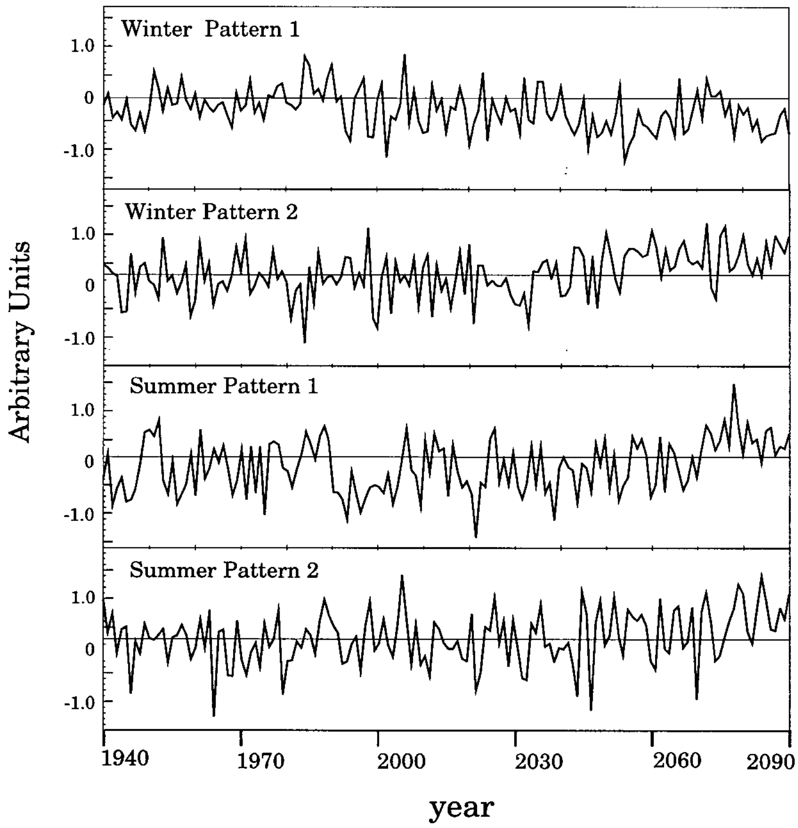

Fig. 10. Seasonal amplitude of the different SLP patterns in the Scenario A integration. The SLP anomalies are referred to the simulated mean annual cycle in the period 1960–1975. The winter patterns are the canonical SLP patterns in Fig. 3. The summer pattern 1 is the canonical SLP pattern in Fig. 6 and the summer pattern 2 is the regression pattern in Fig. 7.

meridional in the summer season. However, the projected changes in the intensity of these SLP patterns does not exceed the level of the internal variability of the climate model (Fig. 10). Otherwise, the validity of the statistical model in the future climate could have been clearly questioned.

The estimated changes in sea-level at the three representative stations 5, 8 and 12 (Fig. 1) along the Chinese coast are shown in Fig. 11. These estimations are obtained by applying the seasonal statistical models to the SLP Scenario A integration, separately for the winter and summer seasons. In order to show more clearly the long-term trends only the respective seasonal means are depicted in this figure, although these time series have been generated on a monthly basis. It can be seen that the estimated future changes are in general small, although one has to be aware that the changes originated in global thermal expansion of water and possible melting of glaciers have to be added up to those estimated by this statistical model, which are caused essentially by the action of wind-stress. Also of interest is the fact that the trends that are observed at the end of the integration may be of different signs for the winter and summer seasons, and for the stations located in the northern or southern stations. In winter the changes of sea-level seem to be negative in the South and positive in the Yellow Sea. In summer, on the other hand, the changes tend to be exactly opposite. This is due to the fact that the atmospheric circulation changes that are relevant for the coastal sea-level also tend to be opposite in summer with respect to

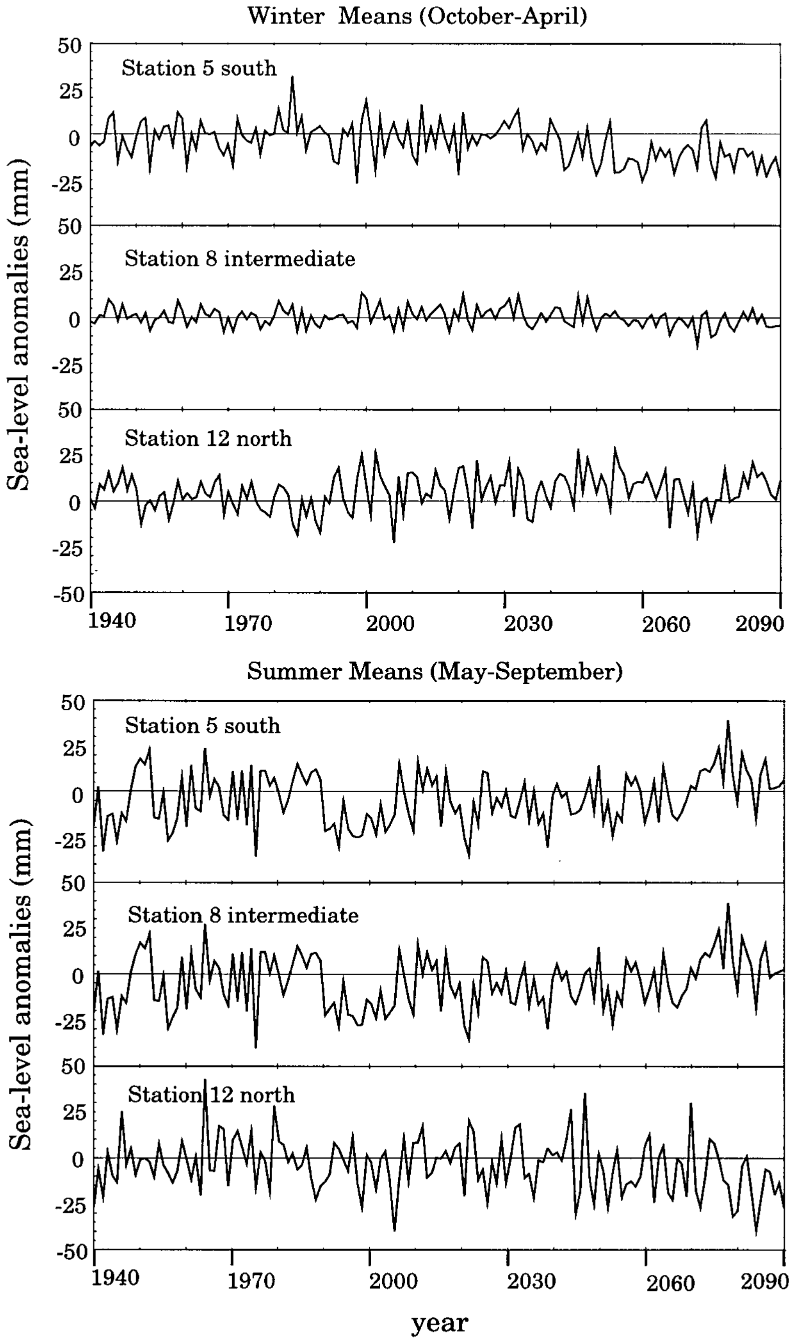

Fig. 11. Estimated coastal sea-level changes along stations 5, 8 and 12 based on the statistical model linking SLP and sea-level and the SLP simulated by the ECHAM1-LSG coupled model forced by IPCC Scenario A greenhouse gas concentrations.

the winter, as explained above. The sea-level in the stations located in intermediate positions are near zero on the long term.

6. Conclusions

The relationships between the large-scale atmospheric circulation and coastal sea-level along the Chinese coast have been statistically analyzed. We have found that a great part of the sea-level variability may be explained generally by the intensities of the meridional and zonal atmospheric circulation over East Asia, although the optimal atmospheric patterns connected to sea-level variability are different for the summer and winter half years.

The physical mechanism that explains these statistical relationships involve the direct piling up of sea-water in the Yellow Sea and larger-scale Ekman pumping along the rest of the Chinese coast. The relationship of sea-level and SST is always weak, so that we conclude that the steric effect plays a minor role in the coastal sea-level variability.

A coupled atmosphere-ocean model integration forced by increasing atmospheric concentration of greenhouse gases according to the IPCC Scenario A has been analyzed in order to estimate the changes of the amplitudes of the SLP patterns that statistical model identifies as relevant for the coastal sea-level variability. It has been found that in this experiment the atmospheric circulation over China by the year 2050 onwards tends to become more zonal in winter and more meridionally oriented in summer.

The implied changes of coastal sea-level are estimated by means of the statistical model fitted with observed data. It is found that the sea-level changes are not very large (of the order of a few centimeters), and that the sign of the changes is opposite in winter and summer, and for the China Sea and for the Yellow Sea. This fact should be important in order to analyze long time series of coastal sea-level, either in this part of the world or elsewhere, to try to detect anthropogenic climate impact on sea-level. If our conclusions are confirmed the sea-level data should be seasonally stratified before undertaking such an analysis.

The IPCC 1995 estimation of mean global sea-level change under the Scenario A assumptions is 49 cm (IPCC, 1996), including the effects of water expansion, glacier melting and changes of the oceanic circulation. On the other hand the effect of changes in the intensity of local processes, such as storms, currents, waves, etc. is much more uncertain. If the results of the coupled climate model can be trusted, the contribution of the atmospheric circulation through wind-stress will probably not be more important than the mentioned factors along the Chinese coast.

7. Acknowledgments

This work was done during a visit of one of the authors, Prof. Cui, to the Institute of Hydrophysics of the GKSS Research Centre in Geesthacht (Germany), that offered financial support and made this visit possible. The National Scientific Fund Committee of China and the Chinese Academy of Sciences contributed, through contract No. 49476274, to collect and pre-analyze the sea-level data. H. von Storch helped us with valuable comments. U. Cubasch made the output of the coupled climate model available to us and K. Arpe kindly provided the sea surface temperature data.

REFERENCES

Bretherton, C. S., Smith C. and Wallace, J. M. 1992. An intercomparison of methods for finding coupled patterns in climate data. *J. Climate* **5**, 541–560.

Cayan, D. 1990. *Variability of latent and sensible heat fluxes over the oceans.* PhD thesis, University of California, San Diego.

Chen X. 1991. Sea level changes since early 1920's from the long records of two tidal gauges in Shanghai. *Quaternary Coastline Changes in China*, 127–141, IGCP-274 China Working Group, Edited by Qin Yunshan and Zhao Zongling.

Cubasch, U., Hasselmann, K. Höck, H. Maier-Reimer, E. Mijolajewicz, U. Santer B. and Sausen, R. 1992. Time-dependent greenhouse gas warming computations with a coupled atmosphere-ocean model. *Clim. Dyn.* **8**, 55–69

Cubasch, U., Hegerl, G. Hellbach, A. Höck, H. Mikolajewicz, U. Santer B. and Boss, V. 1995. A climate change simulation starting at an early time of industrialization. *Clim. Dyn.* **1**1, 71–84.

Cui, M., von Storch H. and Zorita, E. 1995. Coastal sea level and the large-scale climate state: a down-

scaling exercise for the Japanese islands. *Tellus* **47A**, 132–144.
Gill, A. and Niiler, P. P. 1973. The theory of seasonal variability in the ocean. *Deep Sea Research* **20**, 141–177.
Heyen, H., Zorita E. and von Storch, H. 1996. Statistical downscaling of monthly mean North Atlantic air-pressure to sea-level anomalies in the Baltic Sea. *Tellus* **48A**, 312–323.
IPCC, 1990. Climate Change: The IPCC Scientific assessment, Houghton, J. T. Jenkins G. J. and Ephraums J. J. (eds); Cambridge University Press, Cambridge, UK, 365 pp.
IPCC, 1996. Climate Change 1995 — The science of climate change: Contribution of the Working Group I to the 2nd Assessment Report of the Intergovernmental Panel on Climate Change. Hought, J. T. Madeira Filho, L. G. Callander, B. A. Harris, N. Kattenberg A. and Maskell K. (eds). Cambridge University Press.
Lau, K-M, Yang G. J. and Chen, S. H. 1988. Seasonal and intraseasonal climatology of summer Monsoon rainfall over East Asia. *Mon. Wea. Rev.* **116**, 18–37.
Lau, N.-C. 1997. Interactions between global SST anomalies and the midlatitudes atmospheric circulation. *Bull. Amer. Meteor. Soc.* **78**, 21–33.
Lisitzin, E. and Patullo, J. 1961. The principal factors influencing the seasonal oscillation of sea-level. *J. Geophys. Res.* **66**, 845–852.
Mikolajewicz, U., Santer B. and Maier-Reimer, E. 1990. Ocean response to greenhouse gas warming. *Nature* **345**, 1–5.
Patullo, J., Munk, W. Revelle R. and Strong, E. 1955. The seasonal oscillation in sea level. *J. Marine Research* **14**, 88–155.
Tao, S-Y and Chen, L. X. 1987. A review of recent research on the East Asian summer Monsoon in China. In: *Monsoon Meteorology*, Chang C. P. and Krishnamurti T. N. (eds). Oxford University Press, 60–92.
Sahagian, D., Schwartz F. and Kakobs, D. 1994. Direct anthropogenic contribution to sea-level rise in the twentieth century. *Nature* **367**, 54–57.
von Storch, H. 1995. Inconsistencies at the interface between climate research and climate impact studies. *Metereologische Zeitschrift* **4**, 72–80.
von Storch, H., Zorita E. and Cubasch, U. 1993. Downscaling of global climate change estimates to regional scale: an application to Iberian rainfall in wintertime. *J. Climate* **9**, 1161–1171.
Wang, S-W and Zhao, Z-C 1981. Droughts and floods in China 1470–1979. In: *Climate and History*, Wigley, T. M. Ingrasham M. I. and Farmer G. (eds). Cambridge University Press, 271–288.
Warrick, R. A. and Oerlemans, H. 1990. Sea level rise. In: *Climate Change*. The IPCC Scientific Assessment. Hought J. T., Jenkins C. J. and Ephraum J. J. (eds). Cambridge University Press.
Wunsch, C. and Stammer, D. 1997. Atmospheric loading and the inverse barometer effect. *Rev. of Geophys.* **35**, 79–107.
Wyrtki, K., 1990. Sea level rise: the facts and the future. *Pacific Science* **44**, 1–16.